

## Poly (l-lactide acid) improves complete nano-hydroxyapatite bone scaffolds through the microstructure rearrangement

Cijun Shuai<sup>1,2</sup> · Yi Nie<sup>1</sup> · Chengde Gao<sup>1</sup> · Haibo Lu<sup>1</sup> · Huanlong Hu<sup>1</sup> · Xuejun Wen<sup>3</sup> · Shuping Peng<sup>4</sup>✉

1 Central South University, State Key Laboratory of High Performance Complex Manufacturing, Changsha, P.R. China

2 Central South University, State Key Laboratory of Powder Metallurgy, Changsha, P.R. China

3 Medical University of South Carolina, Department of Regenerative Medicine & Cell Biology, Charleston, SC, USA

4 Central South University, Cancer Research Institute, Changsha, P.R. China

✉ Corresponding author: shuping@csu.edu.cn

Received April 13, 2012 / Accepted July 25, 2012

Published online: November 15, 2012

© 2012 by Pontificia Universidad Católica de Valparaíso, Chile

**Abstract** Cracks often occur when nano-hydroxyapatite bone scaffolds are fabricated with selective laser sintering, which affect the performance of scaffolds. In this study, a small amount of poly (l-lactide acid) (PLLA) was added into nano-hydroxyapatite (nano-HAP) powder by mechanical blending in order to improve the sintering properties. The nano-HAP powder combined with 1wt % PLLA was sintered under different laser power (5W, 7.5W, 10W, 12.5W, 15W and 20W). The fabricated scaffolds were characterized using Scanning Electron Microscope (SEM), X-ray Diffraction (XRD), Fourier transform infrared spectroscopy (FT-IR) and Micro Hardness Tester. The results showed that nano-HAP particles grew up quickly with the laser power increasing, and there were many strip-like cracks on the surface of sintering zone. The cracks gradually reduced until disappeared when the laser power increased to 15W, together with a great improvement of density. Large pores were observed on the specimen when the laser power further increases, accompanied with the decomposition of HAP into  $\beta$ -tricalcium phosphate ( $\beta$ -TCP) and tetracalcium phosphate (TTCP). And the optimum parameters were eventually obtained with laser power of 15W, scanning speed of 1000 mm/min, powder bed temperature of 150°C, laser spot diameter of 2 mm and layer thickness of 0.2 mm. We summarized that the molten PLLA enhanced the particle rearrangement of nano-HAP by capillary force and may absorb thermal stress in laser sintering process, while PLLA would be oxidized gradually until completely excluded from the sintered nano-HAP scaffolds, which was confirmed by FTIR analysis. This study provides a novel method to improve the sintering properties of nano-HAP with no adverse effects which would be used in the application of bone tissue engineering potentially.

**Keywords:** hardness, microstructure, nano-hydroxyapatite, thermal properties.

### INTRODUCTION

Hydroxyapatite (HAP) is the main inorganic constituent of natural bone, and possesses a chemical composition similar to human hard tissue (Barralet et al. 2003; Hedia, 2005). It has been considered to be a preferable implantation material due to its excellent biocompatibility in the field of Bone Tissue Engineering (BTE) (Sopyan et al. 2007; Zhou and Lee, 2011).

Selective laser sintering (SLS) can be used to prepare HAP scaffolds owing to its several merits such as suitable for a wide range of materials, high energy density of laser beam, convenient to control etc. (Liu et al. 2007; Shuai et al. 2011a). However, there is a large temperature gradient in sintering zone because of the concentrated energy input, rapid heating and cooling (Ramu and Yadava, 2008; Zhang et al. 2011). It is prone to generate thermal stress and cracks due to the poor thermal conductivity of

HAP (Li et al. 2004; Shuai et al. 2011b). Thus, it is necessary to improve the laser sintering property of HAP in order to acquire a tissue engineer scaffolds with high mechanical and biological performance.

Several groups have reported that polymer matrix can improve the sintering properties of HAP composite. Tan et al. (2003) conducted the sintering experiments with PEEK/HAP (10, 20, 30 and 40wt %) composite to determine the sintering potential of biopolymer with high melting point in the environment of lower temperature. PCL/HAP composite of different percentage weights of HAP (10, 20 and 30wt %) were analyzed for their suitability for fabrication via SLS, as well as the studies of PVA/HAP (10wt % HAP) on bio-composites for bone replacement applications (Wiria et al. 2007; Wiria et al. 2008). Nanocomposite microspheres, prepared by emulsion techniques with 10wt % carbonated hydroxyapatite (CHAP) nanospheres and PLLA microspheres were used to produce scaffolds (Zhou et al. 2008). These methods were proved to improve the laser sintering properties of HAP and fabricate HAP scaffolds with excellent properties. All of above scaffolds are polymer matrix composite in which polymers acts as binder and HAP as reinforcement. However, the presence of polymers in the scaffolds would result in some adverse effects when implanted in vivo, which has been well documented in many literatures.

Poly(L-Lactide)(PLLA,  $(C_6H_8O_4)_n$ ), the polymer of L,L-lactide (also known as L-lactide), has been widely reported to be used in the fields of orthopedic and reconstructive surgery due to its good biodegradation activity (Cretu et al. 2004; Walton and Cotton, 2007; Chen et al. 2010). It degrades by simple hydrolysis of the ester bonds into lactic acid, which is processed through metabolic pathways and is ultimately eliminated from the body, through the respiratory system, as carbon dioxide (von Recum et al. 1995; Weir et al. 2004). However, low cell adhesion to PLLA because of its hydrophobic surface is disadvantageous (Nakagawa et al. 2006). Moreover, PLLA causes inflammatory reactions and foreign-body reactions (Böstman and Pihlajamäki, 2000; Seino et al. 2007; Lee et al. 2010), and its degradation releases oligomers and monomers which involve the possible risk of tumor formation (Yanagida et al. 2009).

In this study, we investigated a strategy to improve the sintering properties of nano-HAP for bone scaffolds by adding a small amount of PLLA (1wt %). The microstructure evolution was studied under different laser power using SEM, FTIR and XRD. The role of small amount of PLLA in enhancing the laser sintering properties of HAP powders was summarized using a novel sintering model.

## EXPERIMENTS

### Materials

The nano-sized HAP powder was purchased from Nanjing Emperor Nano Material Co., Ltd. It was prepared by sol-gel method, with the reaction of trimethyl phosphite  $[(CH_3O)_3P]$  and calcium nitrate  $[Ca(NO_3)_2 \cdot 4H_2O]$ . The purity of HAP is  $\geq 99.5\%$ , while the whiteness of HAP is 96 and pH value is 7.41. The micro-sized PLLA powder was purchased from Jinan Daigang Biomaterial Co., Ltd. It was synthesized by the ring-opening polymerization of lactides under the catalysis of stannous octoate. The glass transition temperature of PLLA is  $60\text{--}65^\circ\text{C}$  and melting temperature is  $175\text{--}185^\circ\text{C}$ . PLLA has a relative molecular mass of 10000, viscosity of 0.51-1.0 dl/g and a purity of  $\geq 99\%$ . The composite powder combined with 99wt % nano-HAP and 1wt % PLLA was served as raw material for the sintering experiment.

### Experimental process

A home-made SLS system was established for fabrication of artificial bone scaffold (Shuai et al. 2010). The laser is a Firestar® t-Series 100W  $CO_2$  Laser manufactured by SYNRAD Co. USA with a maximum output power of 100W. The energy intensity across the laser beam diameter follows the rule of the Gaussian distribution. The laser beam can be focused into a spot with minimum 50  $\mu\text{m}$  in diameter by an optical focus system. The sintered specimens were obtained under different laser power (5W, 7.5W, 10W, 12.5W, 15W and 20W), when other process parameters (Table 1) remain consistent.

**Table 1. The process parameters in the sintering experiment.**

process parameters	value
PLLA (w%)	1
Scan speed (mm/min)	1000
Powder bed temperature (C°)	150
Laser spot diameter (mm)	2
Layer thickness (mm)	0.2
scan interval (mm)	4
distance from the convex lens to the sample (mm)	43.06
dwel time (ms)	120

## Characterization

The morphology and microstructure of the samples was examined with scanning electron microscope (SEM) (JSM-6490LV, JEOL Co. Japan). Each specimen was coated with gold prior to examination. X-ray diffraction analysis (X-RD) was performed using a D8-ADVANCE diffractometer (Bruker Co. German) with  $K\alpha$  radiation ( $\lambda = 1.54056\text{\AA}$ ) over the  $2\theta$  range of  $0-70^\circ$  for the samples. Fourier transform infrared absorption spectra (FT-IR) of the samples were measured in the spectral range of  $400-4000\text{ cm}^{-1}$  using a Nicolette TM 6700 (Thermo Scientific Co. USA). The hardness of nano-HAP scaffolds were measured with Digital Micro Hardness Tester (model HXD-1000TM/LCD) produced by Taiming Optical Instrument Co. China.

## RESULTS

### Morphology and microstructure analysis

The microstructure of initial complete nano-HAP, PLLA and the powder nano-HAP as well as 1wt %, PLLA were shown in Figure 1. The initial complete nano-HAP particles were long needle like with about 150 nm in length and 20 nm in width in Figure 1a. PLLA particles were irregular and an average particle size of 1 to 5  $\mu\text{m}$  in Figure 1b. Nano-HAP particles were embedded among PLLA micro particles evenly in nano-HAP powder combined with 1wt % PLLA by mechanical mixing in Figure 1c. Figure 1a and Figure 1b were taken at magnification factors of 40000 and 5000, respectively in order to show the microstructure of nano-HAP and micro-sized PLLA clearly. We tried different content of PLLA (0, 0.1%, 1%, and 2%) (data not shown), many long cracks appeared in the sintered specimen without PLLA, and the cracks reduced gradually with the increasing of PLLA content, the cracks disappeared completely in sintered specimens when HAP was combined with 1wt % PLLA. However, there were holes when the content of PLLA was over 2wt %, which made it impractical to provide sintering support for scaffold with complex shapes. Therefore, we chose 1wt % PLLA to proceed with the next experiments.

The SEM images of sintered nano-HAP specimens with 1wt % PLLA under different laser power are shown in Figure 2. No obvious morphological changes were observed on the powder layer when laser power was 5W in Figure 2a. It suggested that the laser power was too low to sinter HAP particles. When laser power was 7.5W, PLLA is molten, and HAP particles began to bond with each other through PLLA and there were a lot of sintering necks as well as some pores in Figure 2b. When laser power was 10W, many visible particles boundaries appeared between HAP particles which had regular cylindrical shape in Figure 2c. When laser power was 12.5W, HAP particles grew gradually and distributed randomly in the sintering zone. The density of sintered specimen increased but the pores still existed in Figure 2d. When laser power was 15W, a dense HAP ceramic was obtained (Figure 2e). When laser power is 20W, HAP particles still bond to each other closely in Figure 2f. The magnification factors were different because lower magnification (Figure 2d-e-f) can demonstrate the sintered microstructures at different laser power more clearly. HAP particles grow up rapidly with the increase of laser power.

The macrostructures of the sintered specimens combined by 1wt % PLLA under different laser power are shown in Figure 3. When laser power was 5W, the powder was still loose and smooth. The laser power was too low to melt HAP, while PLLA micro particles which have a lower melting point melted. It

indicated that the HAP particles are not sintered completely under the condition of low surface energy (Figure 3a). When laser power was 7.5W, the powder shrinks but many large and long strip-like cracks occur on the surface of sintering zone, which indicated that the laser power was insufficient (Figure 3b). With the increasing of laser power, HAP particles with enough surface energy began to melt and bond with each other and the cracks in sintered specimens gradually decreased and eventually a dense HAP ceramic was obtained in Figure 3c. When laser power was 12.5W, the cracks decreased and the density of sintered specimen further increased in Figure 3d. When laser power was 15W, the cracks disappeared and the sintered specimen had a high density in Figure 3e. When laser power is 20W, there existed large pores with diameters of about 50-100  $\mu\text{m}$  in the sintered specimen (Figure 3f), which were mainly attributed to the rapid gasification and exclusion of PLLA when laser power is too high (Yen, 2012). When laser power was too high, many big holes existed in the sintered specimen.

### FT-IR analysis

FT-IR spectra of initial complete nano-HAP, PLLA and the nano-HAP combined with 1wt % PLLA is shown in Figure 4 (Kailasanathan and Selvakumar, 2012). The peaks at  $1758\text{ cm}^{-1}$ ,  $1188\text{ cm}^{-1}$ ,  $1455\text{ cm}^{-1}$  represent the vibration of C=O, C-O, and CH(CH<sub>3</sub>) respectively in the spectrum of PLLA (Figure 4a). The broad peaks at  $1091\text{ cm}^{-1}$  and  $1037\text{ cm}^{-1}$  represent the asymmetrical stretching vibration of  $\text{PO}_4^{3-}$ . The peaks at  $961\text{ cm}^{-1}$  are due to symmetrical stretching vibration of  $\text{PO}_4^{3-}$ , and the peaks at  $603\text{ cm}^{-1}$  and  $567\text{ cm}^{-1}$  are assigned to flexural vibration of  $\text{PO}_4^{3-}$ . It was consensus on the bond at  $3563\text{ cm}^{-1}$  and  $630\text{ cm}^{-1}$  due to stretching vibration and flexural vibration of -OH in crystal lattice of nano-HAP, and the peaks at  $3443\text{ cm}^{-1}$  and  $1644\text{ cm}^{-1}$  might be attributed to bond water in FT-IR spectrum of nano-HAP. The weak peaks of  $\text{PO}_4^{3-}$  and -OH at  $1091\text{ cm}^{-1}$  and  $630\text{ cm}^{-1}$  demonstrated that the original nano-HAP had a low crystalline shown in Figure 4b. In the FT-IR spectrum of the nano-HAP combined with 1wt % PLLA, the characteristic peaks of  $\text{PO}_4^{3-}$  and many peaks from  $500\text{ cm}^{-1}$  to  $1400\text{ cm}^{-1}$  of PLLA overlapped, while the absorption peaks of C=O,  $\text{PO}_4^{3-}$ , -OH and bond water did not shift their positions. It seemed that the spectrum in Figure 4c is the superimposing of nano-HAP and PLLA, and no new peaks appeared in this spectrum. This phenomenon demonstrated that no chemical reaction occurred practically between HAP and PLLA.

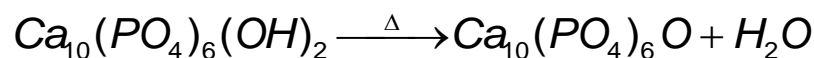
The spectra of the sintered specimens under different laser powers were shown in Figure 5. It was observed that C=O peak at  $1758\text{ cm}^{-1}$  gradually weakened until disappeared with the increase of laser power from 0W to 10W. These changes meant that PLLA particles gradually melted and oxidized in the sintering process. When laser power was 15W, the absorption bond ranged from  $1000\text{ cm}^{-1}$  to  $1100\text{ cm}^{-1}$  of  $\text{PO}_4^{3-}$  was split into two obvious peaks appeared. This phenomenon might be attributed to the presence of  $\text{PO}_4^{3-}$  to crystal lattice of HAP and the change of HAP with high instead of low crystalline. It was also noted that the peaks of -OH at  $3563\text{ cm}^{-1}$  and  $630\text{ cm}^{-1}$  gradually increased in the sintering process. The result indicated the increasing of crystalline of HAP, which was consistent to the results of SEM analysis.

### XRD analysis

XRD analysis is shown in Figure 6. The crystalline peaks of nano-HAP at  $2\theta = 25.80^\circ$ ,  $27.98^\circ$ ,  $28.87^\circ$ ,  $31.69^\circ$ ,  $32.82^\circ$ ,  $33.97^\circ$ ,  $39.76^\circ$  were matched with the JCPDS card 9-432 of nano-HAP. The original nano-HAP particles have a lower crystalline compared with that of the sintered specimen in Figure 6a. The XRD pattern of complete PLLA showed three characteristic peaks at  $2\theta = 14.56^\circ$ ,  $16.52^\circ$ ,  $18.89^\circ$  in Figure 6b. In the XRD pattern of mixture of nano-HAP and 1wt % PLLA, the diffraction peaks of nano-HAP were clear but the peaks of PLLA could not be observed in Figure 6c. This may be due to the too low weight percentage (1wt %) of PLLA in the composite and it was difficult to detect this tiny phase with XRD. However, micro amount of PLLA can be detected by FT-IR analysis. The phenomenon that the crystalline peaks of nano-HAP did not shift confirmed that there was no chemical reaction between nano-HAP and PLLA, which is consistent to the results of FT-IR.

The typical patterns of sintered specimens with the laser power of 5W, 7.5W, 10W, 15W, and 20W were shown in Figure 6d-h. It suggested that the intensities of HAP peaks increased and the peak widths were narrowed down gradually with the increasing of laser power. These changes were attributed to the growth of HAP grain and the increase of its crystalline during the sintering process. When laser power was lower than 15W, there was no shift of the position and quantity of the peaks in each specimen. It suggested that no other phases generated and HAP did not decompose. When laser power was 20W, new peaks occurred in the XRD pattern, which represented the specific characteristic

peaks for  $\beta$ -TCP (#70-0364) and TTCP (#70-1379). This result was assigned to the following decomposition reaction of HAP at high temperature in Equation 1 and Equation 2:



[Equation 1]



[Equation 2]

The relationships between laser power and the hardness of specimens sintered with PLLA are shown in Figure 7 when other processing parameters remain unchanged. It can be seen that the hardness of sintered specimens increased when laser power increased from 10W to 12.5W. But, the hardness of sintered specimens would decrease when laser power increased from 12.5W to 20W. This change was mainly due to the grain growth of HAP while the density of sintered specimens maintained unchanged. Thus, this hardness study had further support to the observation made in SEM and XRD.

## DISCUSSION

Compared with thermally sintered (conventional) process, there is a large temperature gradient between sintering zone and surrounding non-sintered powder owing to the concentrated energy input and the poor thermal conductivity of nano-HAP. Sintering zone is prone to bear the compressive stress of surrounding powder when heated, while a tensile stress when cooled (Matsumoto et al. 2002). Moreover, the temperature of sintering zone will change quickly and dramatically in laser sintering process (Sun and Gupta, 2008). The thermal stress is also caused by the Gaussian distribution of laser beam, which can result in a radial temperature gradient in sintering zone (Gu et al. 2008). The release of thermal stresses can lead to cracks in sintered scaffolds. PLLA was reported to absorb the thermal stresses effectively by introducing transient liquid phase (TLP) in laser sintering process (Li and Yang, 2006). The introduced TLP can wet the surface of HAP particles through viscose flow and lead to rearrangement of HAP particles due to the drag of capillary force  $\sigma$  shown in Equation 3 (Butt and Kappl, 2009) and the surface energy  $P$  of HAP itself (Wakai, 2007). Thus, based on these findings, a model of the interaction between the microstructure evolution of nano-HAP and PLLA was established in Figure 8.

$$\sigma = \gamma \left( \frac{1}{r_1} + \frac{1}{r_2} \right)$$

[Equation 3]

$\gamma$  is the surface tension of liquid-vapor interface,  $r_1$  and  $r_2$  are the curvature radiuses of two curved liquid surfaces.

When sintering temperature reaches the melting point of PLLA, it melts and viscose flow exists in sintering zone. But particles rearrangement cannot occur because the surface energy of HAP particles is insufficient. Thus the molten PLLA can only fill part of gaps between HAP particles and absorb a little thermal stress in sintering zone (Figure 8b). With the increase of sintering temperature, HAP particles will get enough surface energy and experience particle rearrangement due to both the drag of capillary force and surface tension. PLLA can fill the gaps evenly between HAP particles and effectively absorb the thermal stress in sintering zone (Figure 8c). Under laser irradiation, the molten PLLA will gradually be oxidized until disappear finally and HAP particles will bond to each other by grain boundary diffusion until a dense HAP ceramic is obtained in Figure 8d.

## CONCLUDING REMARKS

A strategy of adding a small amount of PLLA (1wt %) into nano-HAP powder was proved to improve the sintering performance of nano-HAP bone scaffolds. No cracks appeared on the surface of the scaffolds and the densification was improved with the laser power of 15W. There were large pores on the specimen, which may be attributed to the rapid gasification and exclusion of PLLA when laser power is too high. It was also found that HAP decomposed into  $\beta$ -TCP and TTCP. Therefore, optimum parameters were eventually obtained. In a summary, the molten PLLA enhanced the particle rearrangement of nano-HAP by capillary force and may absorb thermal stress in laser sintering process, while PLLA would be oxidized gradually until completely excluded from the sintered nano-HAP scaffolds. This study provides a novel method to improve the sintering properties of nano-HAP.

**Financial support:** This work was financially supported by the following funds: (1) The Natural Science Foundation of China (51222506); (2) The foundation for the author of national excellent doctoral dissertation of PR China (201032); (3) Program for New Century Excellent Talents in University (NCET-10-0792); (4) The Fundamental Research Funds for the Central Universities (2011JQ005); (5) Project supported by the Fok Ying-Tong Education Foundation, China (131050); (6) Open Research Fund of State Key Laboratory of Transient Optics and Photonics, Chinese Academy of Sciences; (7) The Open-End Fund for the Valuable and Precision Instruments of Central South University.

## REFERENCES

- BARRALET, J.E.; FLEMING, G.J.P.; CAMPION, C.; HARRIS, J.J. and WRIGHT, A.J. (2003). Formation of translucent hydroxyapatite ceramics by sintering in carbon dioxide atmospheres. *Journal of Materials Science*, vol. 38, no. 19, p. 3979-3993. [\[CrossRef\]](#)
- BÖSTMAN, O. and PIHLAJAMÄKI, H. (2000). Clinical biocompatibility of biodegradable orthopaedic implants for internal fixation: A review. *Biomaterials*, vol. 21, no. 24, p. 2615-2621. [\[CrossRef\]](#)
- BUTT, H.J. and KAPPL, M. (2009). Normal capillary forces. *Advances in Colloid and Interface Science*, vol. 146, no. 1-2, p. 48-60. [\[CrossRef\]](#)
- CHEN, L.; YANG, J.; WANG, K.; CHEN, F. and FU, Q. (2010). Largely improved tensile extensibility of poly (L-lactic acid) by adding poly ( $\epsilon$ -caprolactone). *Polymer International*, vol. 59, no. 8, p. 1154-1161. [\[CrossRef\]](#)
- CRETU, A.; KUCKLING, D. and ADLER, H.-J. (2004). Hydrophilic-hydrophobic polymers based on poly (L-lactide) and poly (2-hydroxyethyl methacrylate). *Materials Science Forum*, vol. 455-456, p. 425-428. [\[CrossRef\]](#)
- GU, D.; SHEN, Y. and WU, X. (2008). Formation of a novel W-rim/Cu-core structure during direct laser sintering of W-Cu composite system. *Materials Letters*, vol. 62, no. 12-13, p. 1765-1768. [\[CrossRef\]](#)
- HEDIA, H.S. (2005). Design of functionally graded dental implant in the presence of cancellous bone. *Journal of Biomedical Materials Research Part B: Applied Biomaterials*, vol. 75B, no. 1, p. 74-80. [\[CrossRef\]](#)
- KAILASANATHAN, C. and SELVAKUMAR, N. (2012). Comparative study of hydroxyapatite/gelatin composites reinforced with bio-inert ceramic particles. *Ceramics International*, vol. 38, no. 5, p. 3569-3582. [\[CrossRef\]](#)
- LEE, B.I.; YOO, J.H.; CHUN, D.I.; CHOI, H.S.; MIN, K.D. and JEEN, Y.M. (2010). Delayed foreign body reaction due to bioabsorbable pins used for femoral fixation in anterior cruciate ligament reconstruction: A case report. *The American Journal of Sports Medicine*, vol. 38, no. 1, p. 176-180. [\[CrossRef\]](#)
- LI, J.F.; LI, L. and STOTT, F.H. (2004). Thermal stresses and their implication on cracking during laser melting of ceramic materials. *Acta Materialia*, vol. 52, no. 14, p. 4385-4398. [\[CrossRef\]](#)
- LI, B. and YANG, M. (2006). Improvement of thermal and mechanical properties of poly (L-lactic acid) with 4,4-methylene diphenyl diisocyanate. *Polymers for Advanced Technologies*, vol. 17, no. 6, p. 439-443. [\[CrossRef\]](#)
- LIU, Z.H.; NOLTE, J.J.; PACKARD, J.I.; HILMAS, G.; DOGAN, F. and LEU, M.C. (2007). Selective laser sintering of high-density alumina ceramic parts. In: *Proceedings of the 35<sup>th</sup> International MATADOR Conference*. (18<sup>th</sup>-20<sup>th</sup> July, 2007, Taipei Taiwan), vol. 14, p. 351-354. [\[CrossRef\]](#)
- MATSUMOTO, M.; SHIOMI, M.; OSAKADA, K. and ABE, F. (2002). Finite element analysis of single layer forming on metallic powder bed in rapid prototyping by selective laser processing. *International Journal of Machine Tools and Manufacture*, vol. 42, no. 1, p. 61-67. [\[CrossRef\]](#)
- MURALITHRAN, G. and RAMESH, S. (2000). The effects of sintering temperature on the properties of hydroxyapatite. *Ceramics International*, vol. 26, no. 2, p. 221-230. [\[CrossRef\]](#)
- NAKAGAWA, M.; TERAOKA, F.; FUJIMOTO, S.J.; HAMADA, Y.; KIBAYASHI, H. and TAKAHASHI, J. (2006). Improvement of cell adhesion on poly (L-lactide) by atmospheric plasma treatment. *Journal of Biomedical Materials Research Part A*, vol. 77A, no. 1, p. 112-118. [\[CrossRef\]](#)
- RAMU, P.M. and YADAVA, V. (2008). Determination of thermal stress distribution in metallic layer during selective laser sintering using finite element method. *International Journal of Manufacturing Technology and Management*, vol. 13, no. 2-3-4, p. 280-296. [\[CrossRef\]](#)
- SEINO, D.; FUKUNISHI, S. and YOSHIYA, S. (2007). Late foreign-body reaction to PLLA screws used for fixation of acetabular osteotomy. *Journal of Orthopaedics and Traumatology*, vol. 8, no. 4, p. 188-191. [\[CrossRef\]](#)

- SHUAI, C.; GAO, C.; NIE, Y.; HU, H.; QU, H. and PENG, S. (2010). Structural design and experimental analysis of a selective laser sintering system with nano-hydroxyapatite powder. *Journal of Biomedical Nanotechnology*, vol. 6, no. 4, p. 370-374. [\[CrossRef\]](#)
- SHUAI, C.; GAO, C.; NIE, Y.; HU, H.; ZHOU, Y. and PENG, S. (2011a). Structure and properties of nano-hydroxyapatite scaffolds for bone tissue engineering with a selective laser sintering system. *Nanotechnology*, vol. 22, no. 28, p. 285703-285712. [\[CrossRef\]](#)
- SHUAI, C.; FENG, P.; GAO, C.; ZHOU, Y. and PENG, S. (2011b). Simulation of temperature field during the laser sintering process of nano-hydroxyapatite powder. *Advanced Materials Research*, vol. 314-316, p. 626-629. [\[CrossRef\]](#)
- SOPYAN, I.; MEL, M.; RAMESH, S. and KHALID, K.A. (2007). Porous hydroxyapatite for artificial bone applications. *Science and Technology of Advanced Materials*, vol. 8, no. 1-2, p. 116-123. [\[CrossRef\]](#)
- SUN, C.N. and GUPTA, M.C. (2008). Laser sintering of ZrB<sub>2</sub>. *Journal of the American Ceramic Society*, vol. 91, no. 5, p. 1729-1731. [\[CrossRef\]](#)
- TAN, K.H.; CHUA, C.K.; LEONG, K.F.; CHEAH, C.M.; CHEANG, P.; ABU BAKAR, M.S. and CHA, S.W. (2003). Scaffold development using selective laser sintering of polyetheretherketone-hydroxyapatite biocomposite blends. *Biomaterials*, vol. 24, no. 18, p. 3115-3123. [\[CrossRef\]](#)
- VON RECUM, H.A.; CLEEK, R.L.; ESKIN, S.G. and MIKOS, A.G. (1995). Degradation of polydispersed poly(L-lactic acid) to modulate lactic acid release. *Biomaterials*, vol. 16, no. 6, p. 441-447. [\[CrossRef\]](#)
- WAKAI, F. (2007). Interplay between surface and grain boundary in sintering. *Materials Science Forum*, vol. 558-559, p. 1029-1034. [\[CrossRef\]](#)
- WALTON, M. and COTTON, N.J. (2007). Long-term *in vivo* degradation of Poly-L-lactide (PLLA) in bone. *Journal of Biomaterials Applications*, vol. 21, no. 4, p. 395-411. [\[CrossRef\]](#)
- WEIR, N.A.; BUCHANAN, F.J.; ORR, J.F. and DICKSON, G.R. (2004). Degradation of poly-L-lactide. Part 1: *In vitro* and *in vivo* physiological temperature degradation. *Proceedings of the Institution of Mechanical Engineers Part H: Journal of Engineering in Medicine*, vol. 218, no. 5, p. 307-319. [\[CrossRef\]](#)
- WIRIA, F.E.; LEONG, K.F.; CHUA, C.K. and LIU, Y. (2007). Poly- $\epsilon$ -caprolactone/hydroxyapatite for tissue engineering scaffold fabrication via selective laser sintering. *Acta Biomaterialia*, vol. 3, no. 1, p. 1-12. [\[CrossRef\]](#)
- WIRIA, F.E.; CHUA, C.K.; LEONG, K.F.; QUAH, Z.Y.; CHANDRASEKARAN, M. and LEE, M.W. (2008). Improved biocomposite development of poly (vinyl alcohol) and hydroxyapatite for tissue engineering scaffold fabrication using selective laser sintering. *Journal of Materials Science: Materials in Medicine*, vol. 19, no. 3, p. 989-996. [\[CrossRef\]](#)
- YANAGIDA, H.; OKADA, M.; MASUDA, M.; UEKI, M.; NARAMA, I.; KITAO, S.; KOYAMA, Y.; FURUZONO, T. and TAKAKUDA, K. (2009). Cell adhesion and tissue response to hydroxyapatite nanocrystal-coated poly (L-lactic acid) fabric. *Journal of Bioscience and Bioengineering*, vol. 108, no. 3, p. 235-243. [\[CrossRef\]](#)
- YEN, H.C. (2012). A new slurry-based shaping process for fabricating ceramic green part by selective laser scanning the gelled layer. *Journal of the European Ceramic Society*, vol. 32, no. 12, p. 3123-3128. [\[CrossRef\]](#)
- ZHANG, J.; LI, D.Y.; QIU, B. and ZHAO, L.Z. (2011). Simulation of temperature field in selective laser sintering on PA6/Cu composite powders. *Advanced Materials Research*, vol. 213, p. 519-523. [\[CrossRef\]](#)
- ZHOU, W.; LEE, S.H.; WANG, M.; CHEUNG, W.L. and IP, W.Y. (2008). Selective laser sintering of porous tissue engineering scaffolds from poly(L-lactide)/carbonated hydroxyapatite nanocomposite microspheres. *Journal of Materials Science: Materials in Medicine*, vol. 19, no. 7, p. 2535-2540. [\[CrossRef\]](#)
- ZHOU, H. and LEE, J. (2011). Nanoscale hydroxyapatite particles for bone tissue engineering. *Acta Biomaterialia*, vol. 7, no. 7, p. 2769-2781. [\[CrossRef\]](#)

#### How to reference this article:

SHUAI, C.; NIE, Y.; GAO, C.; LU, H.; HU, H.; WEN, X. and PENG, S. (2012). Poly (l-lactide acid) improves complete nano-hydroxyapatite bone scaffolds through the microstructure rearrangement. *Electronic Journal of Biotechnology*, vol. 15, no. 6. <http://dx.doi.org/10.2225/vol15-issue6-fulltext-3>

## Figures

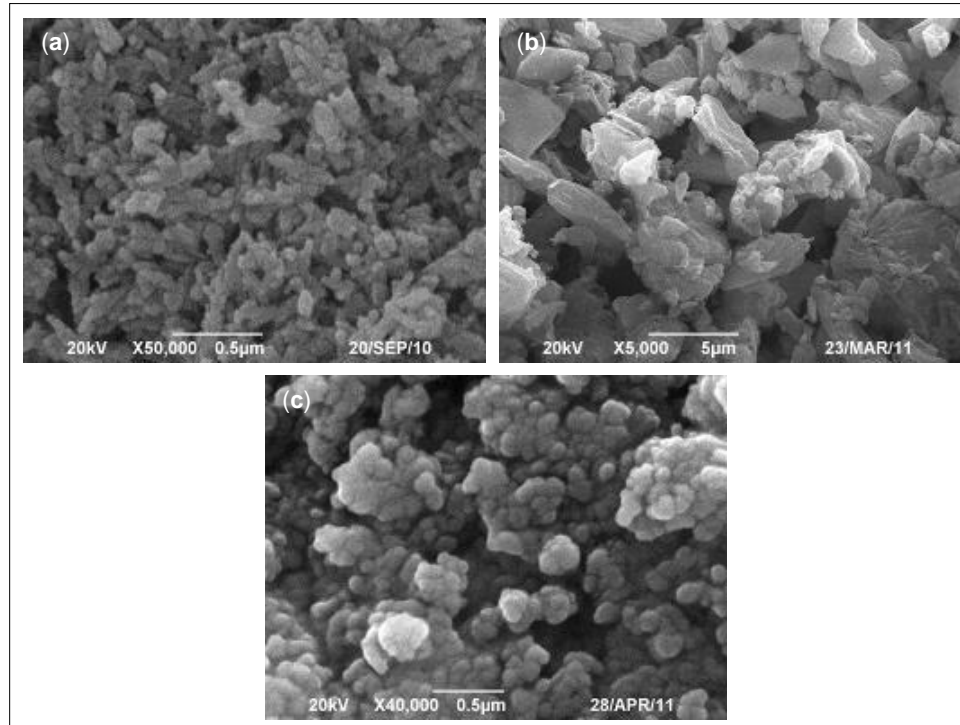


**Fig. 1 SEM micrograph.** (a) initial complete nano-HAP; (b) complete PLLA; (c) nano-HAP combined with 1wt % PLLA.

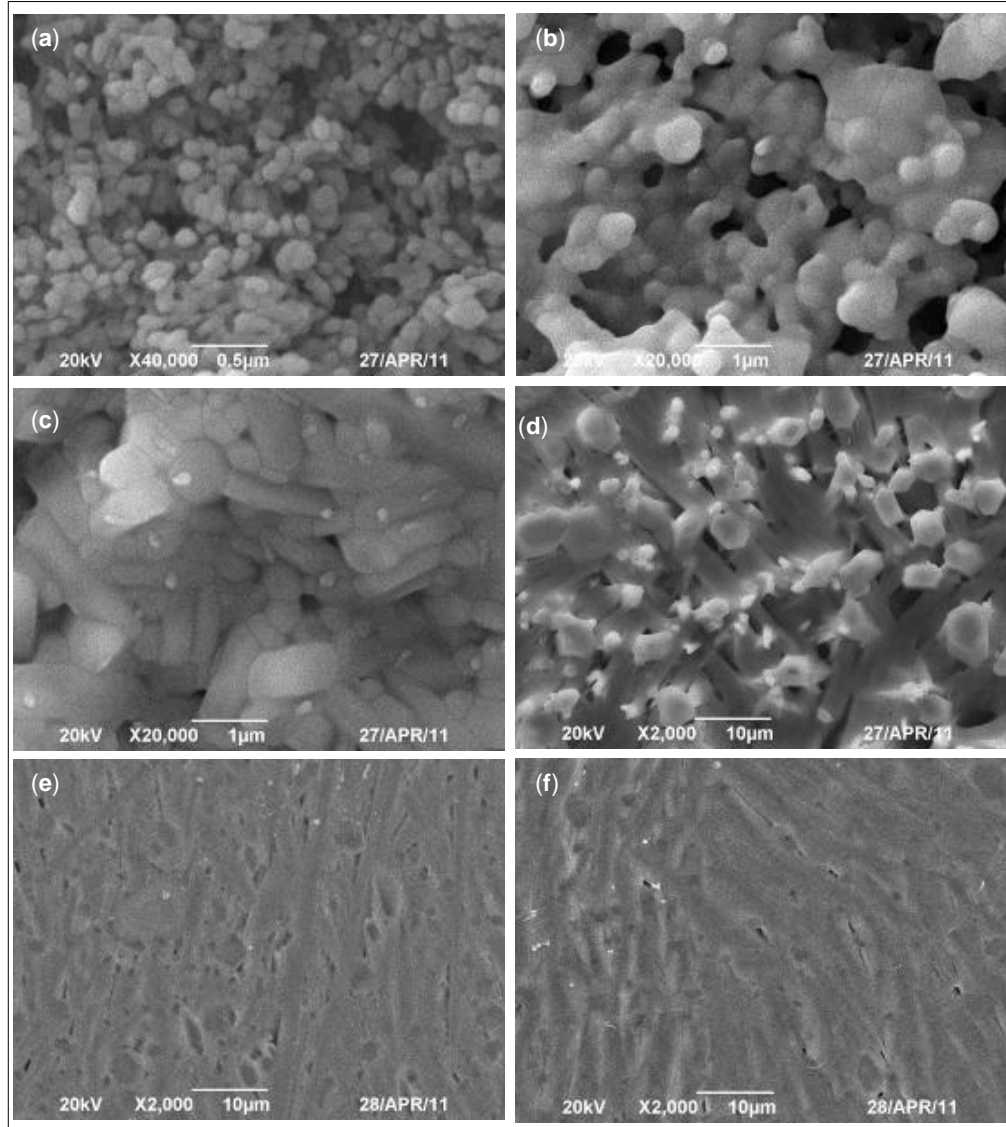


**Fig. 2** The SEM images of sintered nano-HAP specimens by addition of 1wt % PLLA before sintering under different laser power: (a) 5W; (b) 7.5W; (c) 10W; (d) 12.5W; (e) 15W; (f) 20W when other parameters remain consistent.

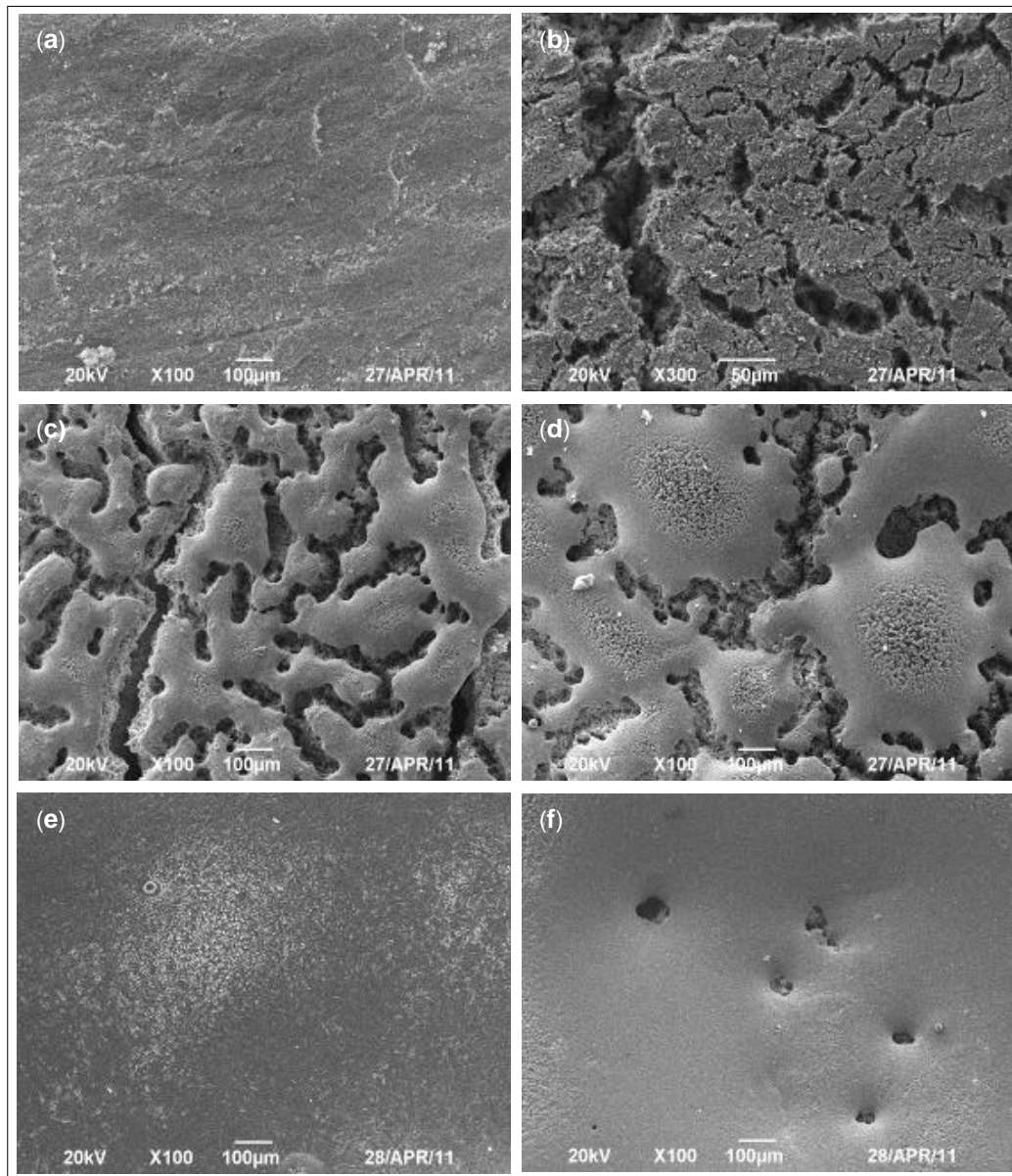


**Fig. 3 SEM macrograph of sintered nano-HAP specimens by addition of 1wt % PLLA before sintering under different laser power: (a) 5W; (b) 7.5W; (c) 10W; (d) 12.5W; (e) 15W; (f) 20W.**

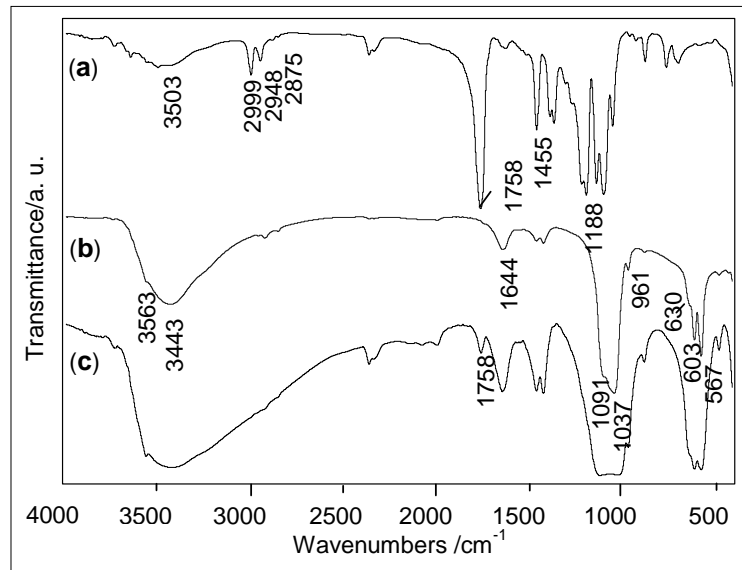


**Fig. 4** FT-IR spectra of initial (a) PLLA; (b) nano-HAP and; (c) nano-HAP specimens by addition of 1wt % PLLA without sintering.

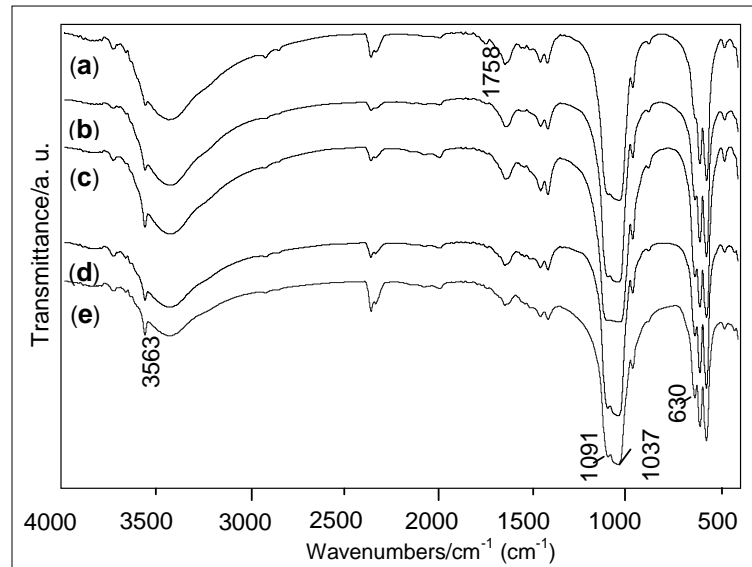


**Fig. 5** FT-IR spectra of nano-HAP specimens by addition of 1wt % PLLA before sintering under different laser power (a) 5W; (b) 7.5W; (c) 10W; (d) 15W and; (e) 20W.

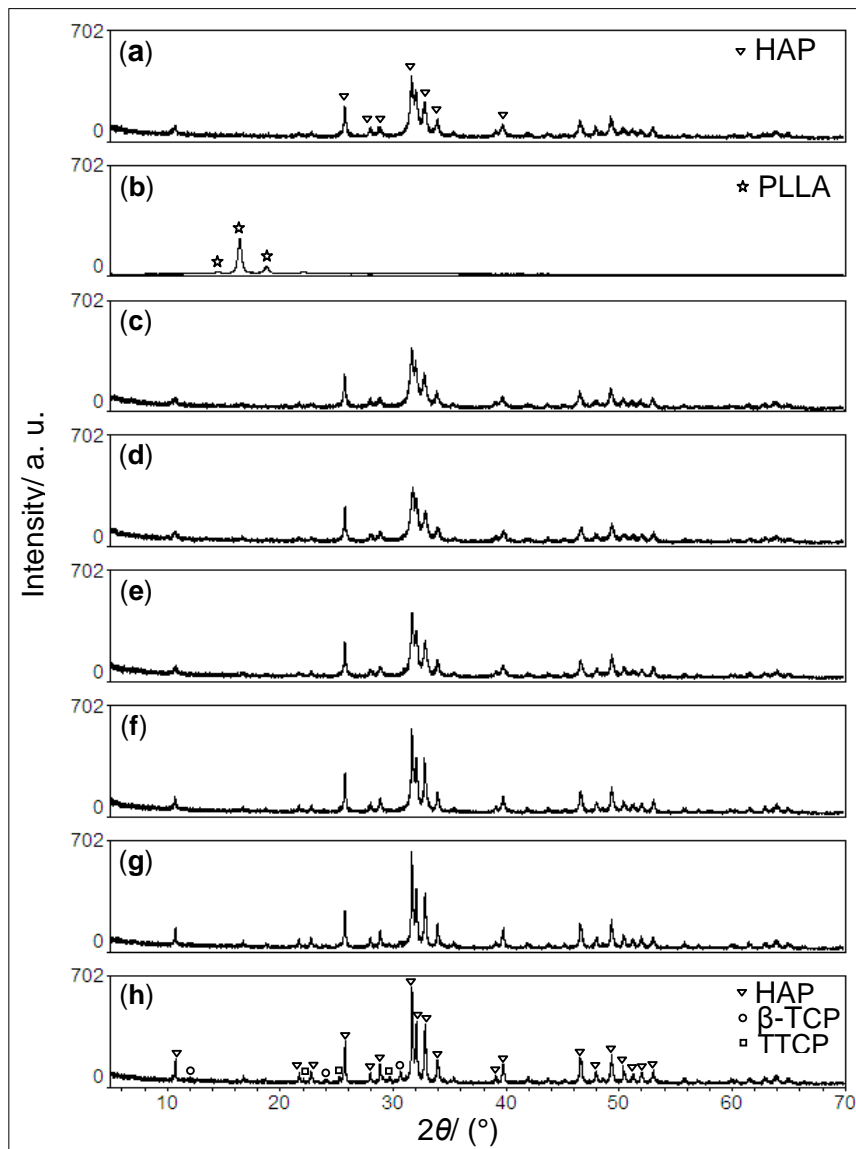


**Fig. 6** XRD pattern of (a) nano-HAP, (b) PLLA, (c-h) nano-HAP specimens by addition of 1wt % PLLA before sintering under different laser power. (c: 0W; d: 5W; e: 7.5W; f: 10W; g: 15W; h: 20W).

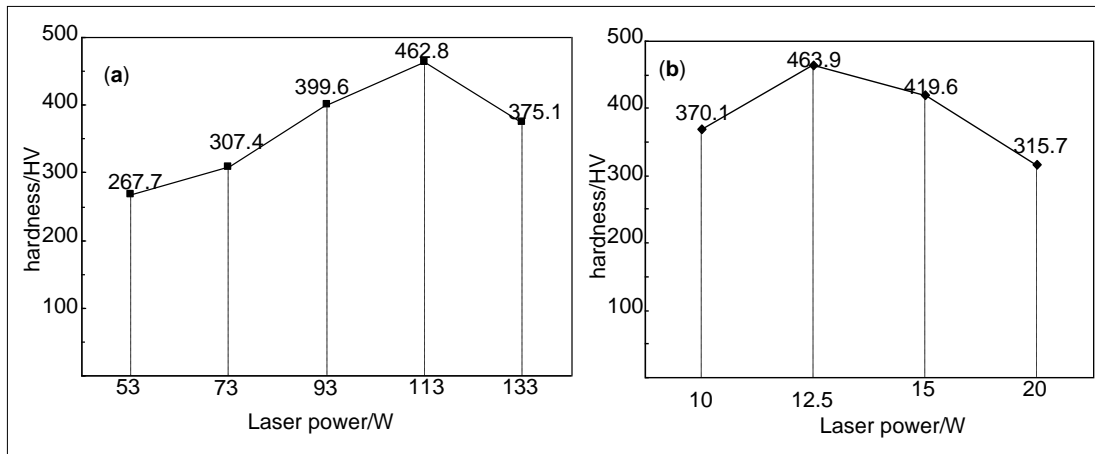


**Fig. 7** Hardness of nano-HAP scaffolds under different laser power. (a) specimens sintered without PLLA; (b) specimens sintered with PLLA.

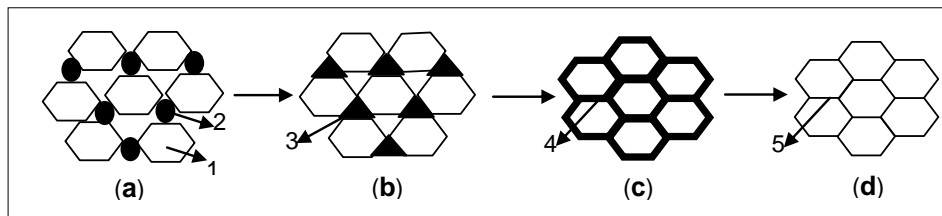


**Fig. 8** Microstructure evolution mechanism on which PLLA affects HAP particles rearrangement. (a) The mixture of nano-HAP with 1wt % PLLA before sintering; (b) sintering temperature reaches the melting point of PLLA; (c) particle rearrangement; (d) HAP particles bind to each other; 1: HAP particles; 2: PLLA; 3: molten PLLA filling part gaps between HAP particles; 4: molten PLLA filling the gaps evenly; 5: grain boundary.